Multi-mode masers of thermally polarized nuclear spins in solution NMR

Vineeth Francis Thalakottoor Jose Chacko,[1] Alain Louis-Joseph,[2] and Daniel Abergel[1,*]

[1] *Laboratoire des Biomolécules, LBM, Département de Chimie, Ecole Normale Supérieure, PSL University, Sorbonne Université, CNRS, 75005 Paris, France*

[2] *Laboratoire de Physique de la Matière Condensée, UMR 7643, CNRS, École Polytechnique , IPP 91120 Palaiseau, France*

We present experimental single and multimode sustained ^{1}H NMR masers in solution on thermally polarized spins at room temperature and 9.4 T achieved through the electronic control of radiation feedback (radiation damping). Our observations illustrate the breakdown of the usual three-dimensional Maxwell-Bloch equations for radiation feedback and a simple toy model of few coupled classical moments is used to interpret these experiments. This work represents a significant step to bring the spontaneous radiation damping based NMR masers in various contexts to the next stage of feedback-controlled and reproducible experiments.

Nonlinearities in nuclear magnetic resonance spectroscopy have attracted much attention in the past decades. Such non conventional behaviours have their origins in cooperative phenomena that involve either the coupling of the spins with the detection circuit - the resonating cavity- in the case of the so-called "radiation damping",[1] or distant dipolar field effects involving the whole sample[2] - a nonlocal phenomenon -, or a combination of both. In high-resolution solution NMR, radiation damping (RD) gives rise to maser induction signals[3, 4] and other unusual effects.[5–11] Strategies have been developed to suppress RD by using field gradients, Q-switching or electronic feedback.[12–15] Radiation feedback may be associated to distant dipolar field effects, leading to even higher complex phenomena[16]. Moreover, sustained NMR masers have also be observed in hyperpolarization experiments in solution, such as ^{129}Xe spin exchange optical pumping experiments, SABRE and PHIP experiments in low and high fields[17, 18], as well as in the context of solid-state dynamic nuclear polarization in liquid helium[19, 20] or in magic-angle spinning experiments.[21] The interplay of radiation damping and the distant dipolar field have also been pinpointed in this context.[22]

The existence of sustained maser pulses caused by radiation damping is quite remarkable and reflects the coexistence of two antagonist phenomena that tend to drive the magnetization to opposite directions along the magnetic field. The radiofrequency back action field from the cavity, slaved to the magnetization, brings the latter to the north pole of the Bloch sphere.[3] To reestablish conditions for the next maser pulse, a second mechanism is therefore required. In low temperature DNP experiments, this ingredient is provided by ongoing negative hyperpolarization of the nuclear spins, opposite to the equilibrium direction.[19, 20] Such sustained masers provided line width reduction by two orders of magnitude in a non rotating solid,[22] and these results also suggested that such an effect could be used to investigate the mechanism of DNP itself.[20] In PHIP and SABRE experiments, spontaneous and efficient RD was shown to give rise to a two-mode maser,[23] and was used to perform measurements of J coupling constants with unprecedented accuracy.[17] In addition, this approach was able to achieve increased sensitivity in some MRI experiments.[24] It was pointed out, however, that in order to achieve the experimental breakthroughs sought for, the proper control of the circuit feedback field is critical to prepare the spins in a precise and reproducible way, i.e., in a state near to the bifurcation state of the dynamical system, where masers are possible.[22]

In this letter, we report the observation of a multi-mode sustained maser in solution NMR at room temperature and generated by an electronic manipulation of the cavity signal.[15] We show that for partially resolved lines, e.g., due to B_0 inhomogeneities, sustained masers with unattenuated steady state are observed, which can be proven by a mathematical analysis to be in contradiction with the usual Maxwell-Bloch equations. Instead, the collective effect of several moments with different Larmor frequencies coupled to the probe, must be treated explicitly.[22, 25] Moreover, a simple toy model of two moments undergoing the same common feedback field from the probe is shown to account for our observations and illustrates the transition from the conventional Maxwell-Bloch behaviour to the actual limit cycle steady state. This work provides better insight into this nonlinear phenomenon and opens new perspectives in complex experimental spin manipulations.

Radiation damping (RD) results from the coupling between a large precessing magnetization and a resonant LC circuit with a high quality factor (Q). The current induced in the detection coil results in a magnetization-dependent feedback field perpendicular to the transverse component. The resulting dynamics is modeled by the well-known Maxwell-Bloch equations,[1, 3, 26] where the magnetization $\mathbf{m}$ is acted upon by a radiation feedback field $\mathbf{B}_{\mathrm{FB}} = Gm(t)e^{-i\psi}$, where $m(t) = \langle m_x \rangle + i\langle m_y \rangle$ is the transverse magnetization. The gain $G = \frac{\mu_o \eta Q}{2}$ and phase $\psi = -\pi/2$

* daniel.abergel@ens.psl.eu

when the NMR detection circuit is tuned to the spins Larmor frequency. It is also possible to generate electronically an "artificial" feedback field that modulates RD by controlling G and ψ.[15] In the presence of an applied rotating radiofrequency field $\mathbf{B_1} = B_1 e^{i(\omega t+\psi_1)}$ with angular frequency ω, the Maxwell-Bloch equation in the rotating frame can be written as:

$$\begin{aligned}\frac{d}{dt}\mathbf{m}(t) &= \gamma\mathbf{m}(t)\times[-(\delta\omega/\gamma)\hat{\mathbf{z}}+\mathbf{B}_1+\mathbf{B}_{\text{FB}}] \\ &- \gamma_2 m(t) - \gamma_1\left[m_z(t)-m_o\right]\hat{\mathbf{z}} \end{aligned} \quad (1)$$

where the offset $\delta\omega = \omega_o - \omega$, γ is the gyromagnetic ratio, γ_1 and γ_2 are longitudinal and transverse relaxation rates. The Maxwell-Bloch equations can be solved only in particular cases[3, 26, 27] but in general require numerical investigations. They are nevertheless amenable to a qualitative analysis,[20, 25, 28] which predicts a sustained maser evolution that eventually leads to a constant transverse amplitude of the magnetization, provided that $m_0 \times \sin\psi > 0$. In usual solution state NMR, where the spins relax to thermal equilibrium ($m_0 > 0$), the feedback field should therefore drives the magnetization towards the $-z$ direction ($\sin\psi > 0$). Alternatively, this necessary condition is also met in hyperpolarization experiments with negative nuclear spins polarization ($m_0 < 0$), where radiation damping brings the magnetization towards the $+z$ direction ($\sin\psi < 0$). This is the case in low temperature DNP,[19, 20, 22] and SABRE[23] experiments.

For several resolved resonance lines, the moments $\mathbf{m}_k$ are tuned to the coil and their contributions to $\mathbf{B}_{\text{FB}}$ have a common ψ, a mild assumption.[29] Therefore, they contribute to the total feedback field $\mathbf{B}_{\text{FB}} = Ge^{-i\psi}\sum_k m_k(t)$, and the modified set of Bloch equations in the rotating frame write as:

$$\begin{aligned}\dot{m}_{xi} &= -\gamma_{2i}m_{xi} - \delta\omega_i m_{yi} + \omega_1\sin\psi_1 m_{zi} - \gamma m_{zi}B_{\text{FB Y}} \\ \dot{m}_{yi} &= \delta\omega_i m_{xi} - \gamma_{2i}m_{yi} - \omega_1\cos\psi_1 m_{zi} + \gamma m_{zi}B_{\text{FB X}} \\ \dot{m}_{zi} &= -\omega_1(\sin\psi_1\, m_{xi} - \cos\psi_1\, m_{yi}) - \gamma_{1i}(m_{zi} - m_{z0i}) \\ &+ \gamma m_{xi}B_{\text{FB Y}} - \gamma m_{yi}B_{\text{FB X}} \end{aligned} \quad (2)$$

where $S_{kx} = \sum_k m_{xk}$, $S_{ky} = \sum_k m_{yk}$, $\mathbf{B}_{\text{FB}} = G\left[\cos\psi S_{kx} + \sin\psi S_{ky}, \cos\psi S_{ky} - \sin\psi S_{kx}, 0\right]^\dagger$, and ω_k and $\delta\omega_k$ are the Larmor frequency and offsets of the magnetization components $\mathbf{m}_k$ in the rotating frame. Equations 2 are the basis for the interpretation of our experimental observations.

The amplitude of the radiation damping field is proportional to the transverse magnetization, to which it lags by 90^{o}. The induction signal can therefore be used to generate a radiation feedback with controlled phase and gain with respect to the transverse magnetization to control the (nonlinear) dynamics of the spins. This was achieved through an electronic feedback control unit (eFCU) that was inspired by a previous design.[15] To this aim, a fraction of the induction signal is picked up through a directional coupler, demodulated using a 400 MHz local oscillator (LO) reference frequency generated from the ^{1}H power amplifier of the spectrometer, filtered and fed back into the probe with adequate phase and gain corrections. Details are given in the Supplemental Material.[30] In particular, this setup is able to invert radiation damping and to drive the magnetization towards the south pole of the Bloch sphere to achieve a solution state NMR maser, in the presence of longitudinal relaxation.

As a first implementation of the device, experiments were performed on a sample containing a 1:1 mixture of methanol and water (225 μL each, 50 μL of deuterated DMSO). Moreover, 20 μL of a 200 mM $CuSO_4$ solution were added to increase transverse relaxation. As a consequence, the CH_3 and OH resonance multiplets were unresolved on the one-dimensional spectrum (see reference spectrum in Supplemental Material). The LO frequency that serves for the quadrature modulation and demodulation in the eFCU was set roughly halfway between the CH_3 and OH ^{1}H resonances (-298.3 Hz and 295.4 Hz from CH_3 and OH, respectively), and the gain and phase of the feedback device were set to rotate the magnetization towards $-z$. In these conditions the signal exhibited initially a few maser bursts of decaying intensities followed by a series of regularly spaced, unattenuated , maser pulses (Fig. 1(a)). This could typically be observed for tens of seconds, and maintained "indefinitely" without damping of the pulse envelope. In this experiment, no pulse was applied to initiate the maser sequence, so that the train of maser pulses occurs after a delay of several tens of ms. This suggests that the sequence is triggered by the circuit noise,[31] since the equilibrium direction is unstable for this set up, or less likely by the weak rf field (4 Hz in this case) leaking from the eFCU device (see SM). The spectrum contains a component at the CH_3 frequency, but also an image resonance line generated by the demodulation/remodulation stages of the eFCU (see SM). The induction signal of the methyl protons is therefore extracted from the spectrum by selecting the resonance line of interest and filtering out the image peak and the rest of the spectrum. An inverse Fourier transform then leads to the pure CH_3 maser induction signal, shown as the orange trace in Fig.1(a). Note that in these experiments, no maser was associated with the OH resonance, which was ascribed to the presence of chemical exchange with water protons.[32, 33]. In this case, spin jumps between sites induce a loss of transverse coherence in a time shorter than the characteristic radiation feedback time, thereby

limiting its efficiency. The absence of an OH signal was confirmed by repeating the same experiment with slightly shifted LO frequencies. Changes of the LO frequency shifted the CH_3 signal image accordingly whilst no additional line at the OH frequency, nor image thereof, were observed (see Fig. SM-3 in the SM). The CH_3 spectrum, shown in Fig.1(c), is composed of lines with alternating intensities and separated by the frequency $1/T$, as expected from the Fourier transform of a periodic signal of period T. It is simply interpreted by remarking that in the case at hand, the NMR signal can be decomposed into two nearly identical waveforms of the same period and shifted in time (see also Eqs.SM-20-SM-22 of the Supplemental Material). The steady-state periodic evolution of the signal is a striking

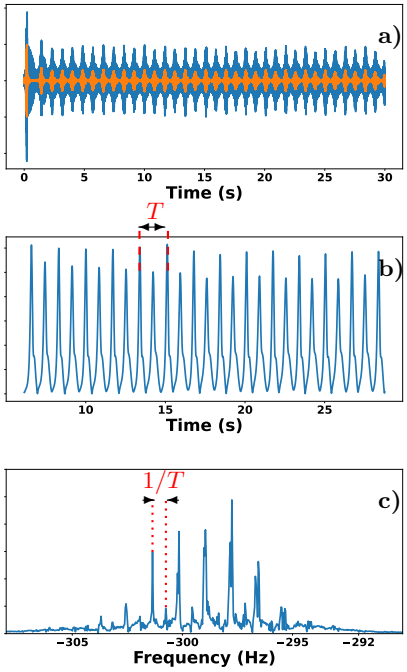

FIG. 1. Sustained maser obtained with the eFCU-controlled radiation feedback. 1(a): ^{1}H signal obtained from a pure methanol sample (blue). The Fourier transform of the induction signal is filtered around the methyl ^{1}H frequency and then back transformed to yield the pure CH_3 ^{1}H maser (orange). 1(b): envelope of the CH_3 ^{1}H maser of the last 25 s of the signal in 1(a). T is the limit cycle period T. The CH_3 ^{1}H line of methanol has a complex pattern resulting from the periodic nature of the NMR signal with an ensemble of spectral lines separated by $1/T$ (1(c)). Experiments were performed on a 400 MHz Bruker spectrometer equipped with triple resonance 5 mm (TXI) probe. Gain and phase were 40 dB and 65.5 deg

feature of this experiment. Indeed, instead of the expected decay of the amplitude of the transverse magnetization towards a stationary value predicted by the Maxwell-Bloch equations, and observed experimentally,[17, 19–21, 23] the envelope of the transverse magnetization oscillates indefinitely, This asymptotic behaviour is the signature of a limit cycle of the dynamical system[34] and implies the existence of a non hyperbolic fixed point of the three-dimensional Maxwell-Bloch equations (i.e., with pure imaginary eigenvalue). However, this is possible only if $\gamma_1 = 0$, in which case the exact analytical solution shows that the magnetization simply evolves towards the z axis,[3] without the possibility of multiple masers. Further details are given in the Supplemental Material. Thus, our observations are at odds with the predictions of the usual three-dimensional Maxwell-Bloch equations. Therefore, a more complex description is necessary to account for the observed non linear dynamics (the "Maxwell" part) of the magnetization.

Experiments were also performed on a sample of pure ethanol (450 μL of ethanol + 50 μL of deuterated DMSO). As in the previous case, the phase and gain of the device were set for radiation feedback inversion and to drive the magnetization towards the $-z$ direction. The local oscillator frequency was set to the center of the CH_3 multiplet. The resulting train of maser pulses, shown in Fig. 2, was Fourier transformed (Fig. 2(b)). The spectrum exhibits resonance lines corresponding to the OH, CH_2, and CH_3 ^{1}H resonances of ethanol (labelled 1, 2, 3). Peaks labelled 4 and 5 are the respective mirror images of the CH_2 and OH signals and are due to the demodulation and re-modulation stages with the reference LO frequency. The latter being set on the CH_3 frequency, no such mirror peak exists for this resonance line. Again, the raw induction signal shows a superposition of regularly spaced and unattenuated maser bursts. This limit cycle kind of behaviour further illustrates the breakdown of the Maxwell-Bloch equations. Disentangling the specific contributions of the different spins from the total signal was simply achieved by back-calculating the time domain signals relative to each resonance line through selective inverse Fourier transform restricted to the spectral

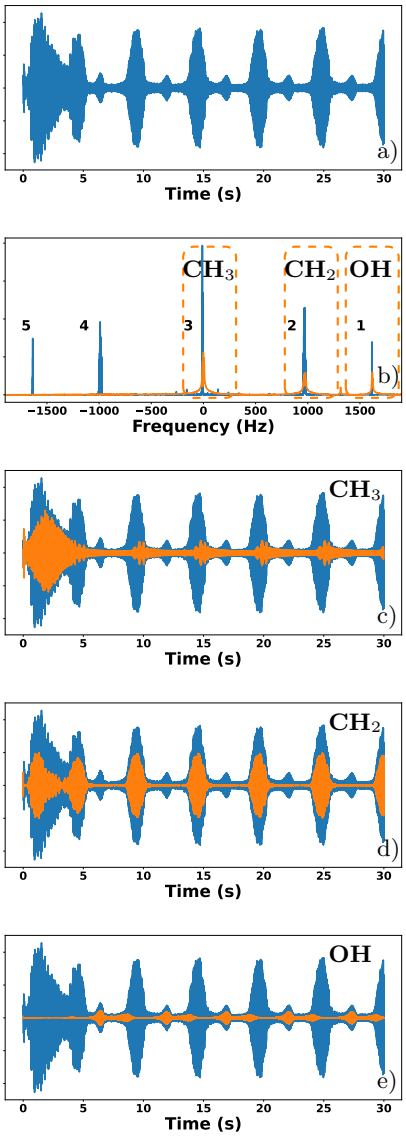

FIG. 2. Sustained multimode maser of ethanol generated by the eFCU. A 30 s multiple maser signal is shown in 2(a). The associated spectrum is shown in 2(b), where peaks 1-3 correspond to OH, CH_2, CH_3. The mirror peaks of 1 and 2 due to quadrature demodulation and re-modulation are labelled 5 and 4 (see text). The 1D spectrum of ethanol obtained in the absence of eFCU is depicted in orange (see also Fig. SM-1 in SM). In 2(c)-2(e), the inverse Fourier transform of the regions corresponding to the CH_3, CH_2 and OH resonance lines of the full spectrum are shown in orange, superimposed with the total induction signal. The gain and phase of the feedback loop were respectively 35 dB and 84.8 deg

region of interest. Each selectively reconstructed induction signal exhibits a series of sustained maser pulses, showing that this experiment produces a three-mode maser built on the radiation feedback of three resolved lines. Moreover, each signal, depicted in Figure 2, evolves toward a periodic steady state maser, meaning that each spin moiety obviously undergoes a stationary limit cycle, as in the case of methanol.

A time-frequency analysis of the induction decays reveals the composite structure of the maser pulses that results from the different magnetization components of the multiplets. In the case of the CH_2 mode, the maser pulses contain contributions at several frequencies that appear shifted in time. In contrast, for the OH maser mode a single frequency is identified, and the shape of the signal is reminiscent of the methanol case, with maser bursts alternatively larger and smaller (see Fig. SM-5 in the Supplemental Material). Besides, the Fourier transform of a single maser burst shows that frequencies tend to cluster in a narrow region of the spectrum that does not reflect the actual multiplet structure and width observed on a simple 1D spectrum (see Fig. 5 in Appendix B). This spectral clustering is a consequence of the nonlocality of the feedback field in the frequency domain expressed by Eq. 2, and can be qualitatively understood

by realizing that when the feedback field dominates the frequency spread of the multiplet, the difference of offset becomes negligible, and the moments tend to undergo the same effective field. These effects are qualitatively well reproduced by simulations (see Fig. SM-6 in the Supplemental Material). In order to understand the inadequacy of the Maxwell-Bloch model for a single moment, we investigated the simplest version of Eqs. 2 consisting of two moments $\mathbf{m}_{1,2}$ subject to radiation feedback. Simulations of this toy model were performed for identical moments m_0 such that $Gm_0 = 7.0$ Hz, relaxation rates $\gamma_1 = 0.2$ s^{-1} and $\gamma_2 = 5$ s^{-1}, and an initial magnetization flip angle = 10^o. The phase of the feedback field was set to $\psi = +\pi/2$.

Results clearly show the transition from the Maxwell-Bloch regime, where the magnetization undergoes a series of monotonously decaying maser bursts and $|m(t)|$ tends to a constant value, to a limit cycle behaviour for $(|m(t)|, m_z(t))$, where the stationary maser *envelope* evolves periodically, a situation that cannot be explained by Eqs. SM-1. Strikingly, this transition occurs even for only a slight offset difference between the moments, whilst both lines remain unresolved ($\Delta\omega/2\pi = 1$ Hz and 1.3 Hz in the simulations - Figs 3(c)-3(d) and 3(e)-3(f)). As expected, the associated spectrum consists of a Dirac comb with lines separated by $1/T$, the period of the maser pulses, and the envelope has the shape of a maser burst. Note that for $\Delta\omega/2\pi = 1.3$ Hz the observed pattern reproduces well the experiment of Fig. 1, and the structure of its Fourier spectrum is the sum of two Dirac combs with a relative phase modulation (for mathematical arguments, see Eqs. SM-20 and SM-22 in the Supplementary Material).

This toy model therefore points to the fact that a structurally different kind of dynamics is expected even in the presence of unresolved, or partially resolved, multiplets. Besides, the qualitative agreement between the methanol maser experiments (Figs. 1(b) -1(c)) and the simulations reported in Figs. 3(e) and 3(f) is noteworthy. The case of methanol, where the CH_3 resonance was completely unresolved is particularly interesting, as in a conventional treatment of NMR radiation feedback, it would be considered as a single magnetization characterized by an effective inhomogeneous transverse relaxation time T_2^*. However, this fails to account for the observed signal, which shows that beyond a mere broadening, field inhomogeneity introduces structural complexity and requires to consider explicitly the effect of several magnetic moments coupled together through a common interaction with the detecting circuit.[25, 35] Consistent with our observations, our simulations show that this phenomenon is essentially contained in a simplistic toy model that is able to account for a dynamics incompatible with the usual Maxwell-Bloch equations. Finally, we

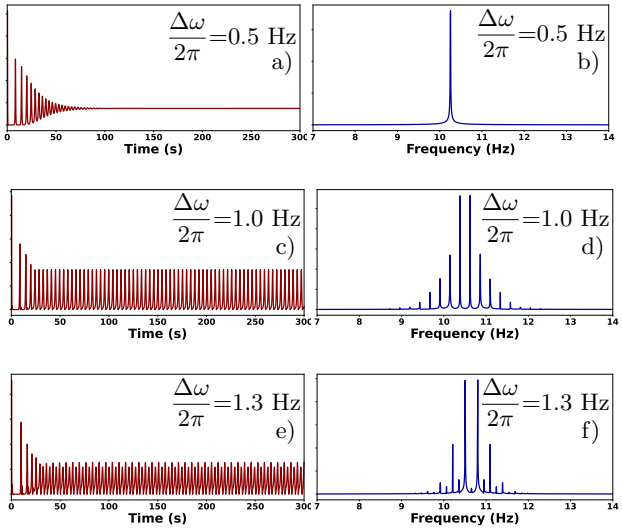

FIG. 3. Amplitude of $m(t)$ and Fourier spectrum of sustained masers for a nonlinear feedback model with two moments. In 3(a) ($\Delta\omega/2\pi = 0.5$ Hz) the magnetization dynamics is analogous to the one predicted by the Maxwell-Bloch equations. In 3(c) ($\Delta\omega/2\pi = 1.0$ Hz) and 3(e) ($\Delta\omega/2\pi = 1.3$ Hz), the stationary evolution is periodic, attesting for the breakdown of the three-dimensional Maxwell-Bloch model. Simulation parameters: $\omega_{\rm FB} = Gm_0 = 7.0$ Hz. The maser is triggered by a 10° initial flip angle.

discuss two limiting cases of the multiple component model that lead to approximate Maxwell-Bloch dynamics. For moments $m_k(t)$ with identical Larmor frequencies $\delta\omega_k = \delta\tilde{\omega}$ and relaxation rates $\gamma_{1,2}$, Eq. 2 (and Eq. SM-8) reduces to the simple Maxwell-Bloch equations where the total feedback field is the sum of identical individual fields and acts on a degenerate line. Alternatively, when all resonance frequency differences $|\delta\omega_i - \delta\omega_k|$ are large, $\sin(\phi_i(t) - \phi_k(t) - \psi)$ and $\cos(\phi_i(t) - \phi_k(t) - \psi)$ are fast varying functions of the time as compared to $a_k(t)$and $m_{zk}(t)$ for all $k \neq i$. Hence,

for $\Delta t >> min(2\pi/|\delta\omega_i - \delta\omega_k|)$, the averages $\bar{a}_i = \frac{1}{\Delta t}\int_{t_0}^{t_0+\Delta t} a(\tau)d\tau$, etc, obey the following relations:

$$\begin{aligned}
\dot{\bar{a}}_i(t) &= -\gamma_{2i}\bar{a}_i - \gamma G m_{zi}(t)\bar{a}_i(t) \\
\dot{\bar{m}}_{zi}(t) &= -\gamma_{1i}(\bar{m}_{zi} - m_{z0i}) + \gamma G \bar{a_i^2}(t)\cos(\psi) \\
\dot{\bar{\phi}}_i(t) &= \delta\omega_i + \gamma G \bar{m}_{zi}(t)\sin\psi,
\end{aligned} \tag{3}$$

which shows that in the case of large offset separations, the moving average for individual magnetizations $\mathbf{m}_i(t)$ also obeys Maxwell-Bloch equations, and each $\mathbf{m}_i(t)$ is decoupled from all other $\mathbf{m}_k(t)$. Thus, in contrast to the former case, the set of moments $\mathbf{m}_i$ behaves as a multimode maser formed by the superposition of single mode masers obeying "averaged" independent sets of Maxwell-Bloch equations. Details of the dynamics for these extreme and intermediate situations are given in the Appendix A

The experiments and discussions presented here provide insight into the manipulation of multimode maser through a controlled radiation feedback field. In order to achieve far reaching - actual [17, 23] and suggested[20] - new applications, it is essential to set the system near to the maser threshold, i.e., near the bifurcation point of the system, in a reproducible manner. In this way, distinct maser modes may remain uncoupled, and additional complex features due to non linearity, including chaotic dynamics, can be avoided. Therefore understanding the details of this Maxwell-Bloch dynamical system with a controllable back action field is of paramount importance to design reliable and reproducible experiments, which are hardly achievable by spontaneous masers. This work represents a significant step in this direction.

Acknowledgements: The authors acknowledge the support of the Agence Nationale pour la Recherche (ANR), Grant ANR-22-CE29-0006-01–DynNonlinPol.

[1] N. Bloembergen and R. V. Pound, Radiation damping in magnetic resonance experiments, Phys. Rev. **95**, 8 (1954).
[2] G. Deville, M. Bernier, and J. M. Delrieux, Nmr multiple echoes observed in solid ^{3}He, Phys. Rev. B **19**, 5666 (1979).
[3] S. Bloom, Effects of radiation damping on spin dynamics, Journal of Applied Physics **28**, 800 (1957).
[4] A. Szöke and S. Meiboom, Radiation damping in nuclear magnetic resonance, Phys. Rev. **113**, 585 (1959).
[5] M. A. McCoy and W. S. Warren, Three-quantum nuclear magnetic resonance spectroscopy of liquid water: Intermolecular multiple-quantum coherence generated by spin–cavity coupling, The Journal of Chemical Physics **93**, 858 (1990), https://pubs.aip.org/aip/jcp/article-pdf/93/1/858/18987030/858_1_online.pdf.
[6] D. Abergel, M. A. Delsuc, and J. Lallemand, Comment on: Is multiple quantum nuclear magnetic resonance spectroscopy of liquid water real?, The Journal of Chemical Physics **96**, 1657 (1992), https://pubs.aip.org/aip/jcp/article-pdf/96/2/1657/18996930/1657_1_online.pdf.
[7] D. Abergel and J. Lallemand, Some microscopic aspects of radiation damping in nmr, Journal of Magnetic Resonance, Series A **110**, 45 (1994).
[8] H. Barjat, G. P. Chadwick, G. A. Morris, and A. G. Swanson, The behavior of multiplet signals under "radiation damping" conditions. i. classical effects, Journal of Magnetic Resonance, Series A **117**, 109 (1995).
[9] X. an Mao, J. xin Guo, and C. hui Ye, Radiation damping effects on spin—lattice relaxation time measurements, Chemical Physics Letters **222**, 417 (1994).
[10] G. Ball, G. Bowden, T. Heseltine, M. Prandolini, and W. Bermel, Radiation damping artifacts in 2d cosy nmr experiments, Chemical Physics Letters **261**, 421 (1996).
[11] P. Pelupessy, Radiation damping strongly perturbs remote resonances in the presence of homonuclear mixing, Magnetic Resonance **3**, 43 (2022).
[12] V. Sklenar, Suppression of radiation damping in multidimensional nmr experiments using magnetic field gradients, Journal of Magnetic Resonance, Series A **114**, 132 (1995).
[13] C. Anklin, M. Rindlisbacher, G. Otting, and F. Laukien, A probehead with switchable quality factor. suppression of radiation damping, Journal of Magnetic Resonance, Series B **106**, 199 (1995).
[14] P. Broekaert and J. Jeener, Suppression of radiation damping in nmr in liquids by active electronic feedback, Journal of Magnetic Resonance, Series A **113**, 60 (1995).
[15] A. Louis-Joseph, D. Abergel, and J.-Y. Lallemand, Neutralization of radiation damping by selective feedback on a 400 mhz nmr spectrometer, Journal of Biomolecular NMR **5**, 212–216 (1995).
[16] Y.-Y. Lin, N. Lisitza, S. Ahn, and W. S. Warren, Resurrection of crushed magnetization and chaotic dynamics in solution nmr spectroscopy, Science **290**, 118 (2000), https://www.science.org/doi/pdf/10.1126/science.290.5489.118.
[17] M. Suëfke, S. Lehmkuhl, A. Liebisch, B. Blümich, and S. Appelt, Para-hydrogen raser delivers sub-millihertz resolution in nuclear magnetic resonance, Nature Phys https://doi.org/10.1038/nphys4076 (2017).
[18] A. N. Pravdivtsev, F. D. Sönnichsen, and J.-B. Hövener, Continuous radio amplification by stimulated emission of radiation using parahydrogen induced polarization (phip-raser) at 14 tesla, ChemPhysChem **21**, 667 (2020), https://chemistry-europe.onlinelibrary.wiley.com/doi/pdf/10.1002/cphc.201901056.

[19] P. Bösiger, E. Brun, and D. Meier, Solid-state nuclear spin-flip maser pumped by dynamic nuclear polarization, Phys. Rev. Lett. **38**, 602 (1977).

[20] E. M. M. Weber, D. Kurzbach, and D. Abergel, A dnp-hyperpolarized solid-state water nmr maser: observation and qualitative analysis, Phys. Chem. Chem. Phys. **21**, 21278 (2019).

[21] M. A. Hope, S. Björgvinsdóttir, C. P. Grey, and L. Emsley, A magic angle spinning activated 17o dnp raser, The Journal of Physical Chemistry Letters **12**, 345 (2021), pMID: 33355469, https://doi.org/10.1021/acs.jpclett.0c03457.

[22] V. F. T. J. Chacko and D. Abergel, Dipolar field effects in a solid-state nmr maser pumped by dynamic nuclear polarization, Phys. Chem. Chem. Phys. **25**, 10392 (2023).

[23] S. Appelt, S. Lehmkuhl, S. Fleischer, B. Joalland, N. M. Ariyasingha, E. Y. Chekmenev, and T. Theis, Sabre and php pumped raser and the route to chaos, Journal of Magnetic Resonance **322**, 106815 (2021).

[24] S. Lehmkuhl, S. Fleischer, L. Lohmann, M. S. Rosen, E. Y. Chekmenev, A. Adams, T. Theis, and S. Appelt, Raser mri: Magnetic resonance images formed spontaneously exploiting cooperative nonlinear interaction, Science Advances **8**, eabp8483 (2022), https://www.science.org/doi/pdf/10.1126/sciadv.abp8483.

[25] D. Abergel, A. Louis-Joseph, and J.-Y. Lallemand, Self-sustained Maser oscillations of a large magnetization driven by a radiation damping-based electronic feedback, The Journal of Chemical Physics **116**, 7073 (2002), https://pubs.aip.org/aip/jcp/article-pdf/116/16/7073/10838953/7073_1_online.pdf.

[26] A. Vlassenbroek, J. Jeener, and P. Broekaert, Radiation damping in high resolution liquid NMR: A simulation study, The Journal of Chemical Physics **103**, 5886 (1995), https://pubs.aip.org/aip/jcp/article-pdf/103/14/5886/9435958/5886_1_online.pdf.

[27] T. M. Barbara, Integration of bloch's equations with radiation damping, Journal of Magnetic Resonance **98**, 608 (1992).

[28] D. Abergel, A. Louis-Joseph, and J.-Y. Lallemand, On the possibility of performing self-calibrated selective $\pi/2$ pulses in nuclear-magnetic resonance, The Journal of Chemical Physics **112**, 6365 (2000), https://pubs.aip.org/aip/jcp/article-pdf/112/14/6365/10804759/6365_1_online.pdf.

[29] M. Guéron, A coupled resonator model of the detection of nuclear magnetic resonance: Radiation damping, frequency pushing, spin noise, and the signal-to-noise ratio, Magnetic Resonance in Medicine **19**, 31 (1991), https://onlinelibrary.wiley.com/doi/pdf/10.1002/mrm.1910190104.

[30] V. T. J. Chacko, *Non-Linearities in DNP-Hyperpolarized Solids at Cryogenic Temperatures*, Ph.D. thesis, Sorbonne Université (20223).

[31] M. P. Augustine, S. D. Bush, and E. L. Hahn, Noise triggering of radiation damping from the inverted state, Chemical Physics Letters **322**, 111 (2000).

[32] J.-H. Chen and X.-A. Mao, Radiation damping transfer in nuclear magnetic resonance experiments via chemical exchange, The Journal of Chemical Physics **107**, 7120 (1997), https://pubs.aip.org/aip/jcp/article-pdf/107/18/7120/19247782/7120_1_online.pdf.

[33] J. C. Rodríguez, P. A. Jennings, and G. Melacini, Effect of chemical exchange on radiation damping in aqueous solutions of the osmolyte glycine, Journal of the American Chemical Society **124**, 6240 (2002), pMID: 12033843, https://doi.org/10.1021/ja0256966.

[34] J. Guckenheimer and P. Holmes, *Nonlinear Oscillations, Dynamical Systems, and Bifurcations of Vector Fields*, Applied Mathematical Sciences No. 42 (Springer, 1983).

[35] D. Abergel and A. Louis-Joseph, Generating spin turbulence through nonlinear excitation in liquid-state nmr, Journal of Magnetic Resonance **196**, 115 (2009).

END MATTER

A.

These limiting cases can be reproduced with numerical simulations for two moments with varying offset separations $\Delta\omega$. For a small $\Delta\omega$ and unresolved lines, the total transverse magnetization $m(t)$ indeed exhibits the usual series of maser pulses with monotonous amplitude decay with an envelope decays to a constant value, in line with the usual Maxwell-Bloch equations. A similar behaviour is observed for large offset difference, where both moments reach similar steady state amplitudes, with an amplitude decay akin to the usual Maxwel-Bloch predictions. However, in the steady state, the amplitudes are not constant and are modulated at a frequency close to the offset difference, larger at small $\Delta\omega$, and hardly visible for large $\Delta\omega$.

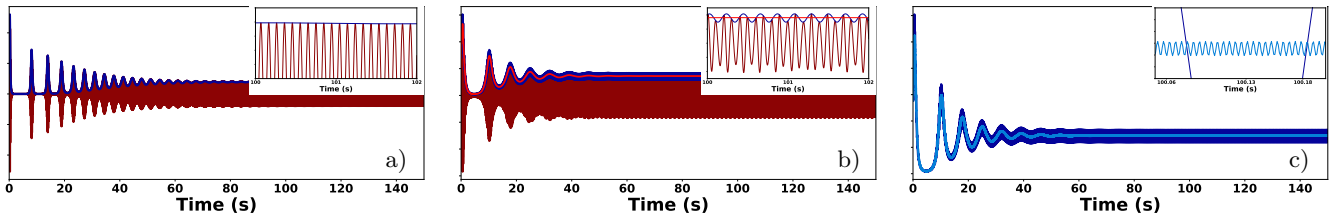

FIG. 4. Departure from the Maxwell-Bloch equations for the two-moment toy model of radiation feedback. Simulations are performed for moments with $\delta\omega_1/2\pi = 10$ Hz and $\delta\omega_2/2\pi = 10.5$ (a),15 (b), and 200 Hz. Only the traces corresponding to the moment at $\delta\omega_1/2\pi = 10$ Hz is shown. The transverse component m_{1x} is depicted in brown. The red trace shows the envelope obtained from the back calculated transverse magnetization from the filtered Fourier spectrum. In (c), the dark and light blue traces correspond to the amplitude $a_1(t)$ for $\delta\omega_2/2\pi = 15$ Hz and $\delta\omega_2/2\pi = 200$ Hz.

This is illustrated in Fig. 4. Limiting cases of Eq.2 are illustrated in Fig. 4 for two moments with different offset separations $\Delta\omega$. For a small $\Delta\omega/2\pi = 0.5$ Hz (Figure 4(a)), therefore unresolved lines, the total transverse magnetization $m(t)$ exhibits the usual series of maser pulses with monotonous amplitude decay (brown trace) while its envelope (dark blue) decays to a stationary value, in line with the usual Maxwell-Bloch equations. When $\Delta\omega/2\pi = 5$ Hz (Figure 4(b)), $\mathbf{m}_1(t)$ still exhibits a series of decaying maser bursts (brown). However, the number of these decreases before a steady state is reached, which is associated to a steady state oscillation of the total transverse magnetization $m(t)$ (dark blue). Finally, the comparison of the decay profiles of the maser bursts for large and small offset differences in Figure 4(c) ($\Delta\omega/2\pi = 190$ Hz and $\Delta\omega/2\pi = 5$ Hz), shows that the amplitudes of $|\mathbf{m}_1(t)|$ are similar in both cases. However, both traces show different steady state modulation of the amplitude $a_1(t)$ that is much slower and much larger for small $\Delta\omega$, where it closely matches the offset difference. In contrast, for large $\Delta\omega$, this modulation is fast and hardly visible, thereby illustrating the Maxwell-Bloch behaviour of the average magnetization expected from Eqs. 3. Interestingly, these oscillations are absent in the analysis of our experiments, as the strategy allowing to identify the distinct masers is based on the filtering of the spectrum around individual resonances followed by an inverse Fourier transform. This amounts to a convolution of the time signal with a time windowing function that averages out the fast variations due to the phase difference between the moments, which is similar in nature to the moving average process described in Eq. 3. As a result, the time domain signal $m(t)$ actually reaches a constant value, rather than an oscillating steady state.

B.

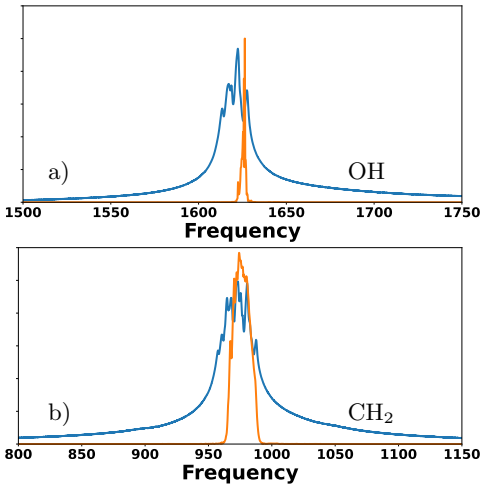

FIG. 5. Spectral clustering in the three-mode ethanol maser. The Fourier transform of a single maser pulse (5(a)-5(b)) exhibits narrower spectral clustering motif for OH (14.46 Hz) than for CH_2 (29.81 Hz). The magnitude spectra are shown in orange, and superimposed to the 1D spectra (in blue).